



JIMMA UNIVERSITY

JIMMA INSTITUTE OF TECHNOLOGY

FACULTY OF MATERIALS SCIENCE AND ENGINEERING

CHAIR OF MATERIALS SCIENCE AND ENGINEERING

MASTERS OF SCIENCE PROGRAM IN MATERIALS SCIENCE
AND ENGINEERING

**Computational study of the effects of silicon doping on
structural, electronic and the born effective charge properties
of monoclinic HfO₂ ferroelectric material**

By: Tseganesh Gensa Geta

A Thesis Submitted to School of Graduate Studies of Jimma University in Partial
Fulfillment of the Requirements of Masters of Science Degree in Materials Science
and Engineering

Nov 2022

Jimma, Ethiopia

JIMMA UNIVERSITY
JIMMA INSTITUTE OF TECHNOLOGY
FACULTY OF MATERIALS SCIENCE AND ENGINEERING
CHAIR OF MATERIALS SCIENCE AND ENGINEERING
MASTERS OF SCIENCE PROGRAM IN MATERIALS SCIENCE
AND ENGINEERING

**Computational study of the effects of silicon doping on
structural, electronic and the born effective charge properties
of monoclinic HfO₂ ferroelectric material**

By: Tseganesh Gensa Geta

A Thesis Submitted to School of Graduate Studies of Jimma University in Partial
Fulfillment of the Requirements of Masters of Science Degree in Materials Science
and Engineering

Main advisor: Dr. Muluaem Abebe (Ph.D.)

Co-advisor: Dr. Solomon Demiss (PhD)

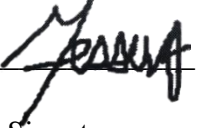
Nov 2022
Jimma, Ethiopia

JIMMA UNIVERSITY
SCHOOL OF GRADUATE STUDIES
JIMMA INSTITUTE OF TECHNOLOGY
FACULTY OF MATERIALS SCIENCE AND ENGINEERING
CHAIR OF MATERIAL SCIENCE AND ENGINEERING
MASTERS OF SCIENCE PROGRAM IN MATERIAL SCIENCE AND ENGINEERING

Computational study of the effects of silicon doping on structural, electronic and the born effective charge properties of monoclinic HfO₂ ferroelectric material

BY: TSEGANESH GENSA GETA

Approved by Board of Examiners:

Dr.Tessera Alemeneh (PhD)		<u>19/ 04/ 2015</u> E.C
External Examiner	Signature	Date
Dr.Himanshu Panjiar (PhD)	_____	___/___/___
Internal Examiner	Signature	Date
Dr.Dhakshnamoorthy Mani (PhD)	_____	___/___/___
Chairperson	Signature	Date
Dr.Mulualem Abebe (PhD)	_____	___/___/___
Main Advisor	Signature	Date
Dr.Solomon Demiss (PhD)	_____	___/___/___
Co-Advisor	Signature	Date

A. DECLARATION

I, Tseganesh Gensa Geta, declare that this MSc thesis entitled “computational study of the effects of silicon doping on structural, electronic and born effective charge properties of HfO₂” has been compiled by me under the supervision of Dr. Mulualem Abebe and that no portion of this work referred to the work has been submitted in support of an application for another degree or qualification of this or any other university or other learning institutes. Except where states or otherwise, are fully acknowledged in accordance with the standard referencing practices, the work presented here is entirely my own.

	Name	Signature	Date
Candidate	Tseganesh Gensa Geta	_____	___/___/___

As master research advisor, we here by certify that we have read and evaluate this MSc research under our guidance by Tseganesh Gensa Geta entitled “computational study of the effects of silicon doping on structural, electronic and born effective charge properties of HfO₂”

We recommended that it can be submitted as fulfilling for MSc. Thesis requirement.

	Name	Signature	Date
1. Main advisor	Dr.Mulualem Abebe (PhD)	_____	___/___/___
2. Co-advisor	Dr. Solommon Demiss (PhD)	_____	___/___/___

B.ABSTRACT

In this study, the structural, electronic, and born-effective charge properties of silicon (Si) doped were investigated with respect to density functional theory by using the Quantum Espresso Package. The local density approximation (LDA) and the generalized gradient approximation (GGA) were used to compute the exchange correlation energy. The total minimum energy of hafnium oxide is determined as a function of cutoff energy and Monk Horst-Pack grid size. The results show that the total minimum energy per atom is monotonically decreasing with increasing cutoff energy due to the variational principle. The total minimum energy is converged at the 5 X 5 X 5 k-point cutoff 35 Rydberg and Monk horst-pack mesh. Furthermore, the lattice parameter is taken from the literature. Our materials' lattice parameters are $a = 5.14\text{\AA}$, $b = 5.19\text{\AA}$, and $c = 5.32\text{\AA}$. This result is in good agreement with the experimental value. Finally, structural, electronic, and born-effective charge properties are calculated for pure and silicon-doped hafnium oxide. The results show that after silicon dope, the band is changed from indirect band gap to direct band gap, and the value of the band gap is decreased because of lattice distortion after silicon dope. One hafnium atom is substituted by a silicon atom because hafnium is more stable than oxygen. The doped-born effective charge shows a large value when we compare with pure hafnium oxide, and it makes a great contribution to the dielectric response.

Keywords: *born effective charge, density functional theory, electronic, silicon, total energy*

C.ACKNOWLEDGEMENT

First and foremost, I would like to thank the Almighty God for giving me this time, strength, and wisdom to complete this thesis work.

Secondly, I would like to express my sincere gratitude to my supervisor, Dr. Muluaem Abebe (PhD), for his continuous support of my MSc thesis and for his patience, motivation, and immense knowledge. His guidelines helped me throughout the research and writing of this thesis. I would also like to thank Wolaita Sodo University for giving me this chance. I am grateful to the School of Material Science and Engineering for their willingness to use their computer facilities in the computational laboratory.

I would like to thank my co-advisor, Dr. Solommon Demiss (PhD), who has accepted me to work with him and who is always ready to support me.

I would like to thank Mr. Dita Deme, who has guided me through collecting supportive materials for my thesis.

Last but not least, I would like to thank my parents for their support and care for me throughout my education. Their support has been invaluable, and it is the reason I have succeeded to where I am today as a person.

Table of Contents

A. DECLARATION	I
B.ABSTRACT	II
C.ACKNOWLEDGEMENT	III
D. LIST OF FIGURES	VI
E. LIST OF ACRONYMS	VII
CHAPTER-ONE.....	1
INTRODUCTION	1
1.1 General background	1
1.2 Hafnium Oxide Overview.....	3
1.3 Dielectric properties and Energy storage	6
1.4 Environmental Influences on Ferroelectric Materials.....	7
1.4.1 Temperature	7
1.4.2 Grain Size.....	9
1.5 Statement of the problem	9
1.6 Objectives of the research	10
1.6.1 General objective	10
1.6.2 Specific objectives	10
1.7 Significance of the study.....	11
1.8 Scope of the study.....	11
CHAPTER -TWO.....	12
LITERATURE REVIEW	12
2.1 Overview of Ferroelectric Materials.....	12
2.2 Conceptual Framework.....	13
2.3 DFT Study of Hafnium Oxide	14
2.4 Application of HfO ₂ Ferroelectric material	14
CHAPTER -THREE.....	16
METHODOLOGY	16
3.1 Methods.....	16

3.2 Computational methodology.....	16
3.3 Electronic structure calculation.....	18
3.3.1 Exchange-correlation energy	20
3.3.2 K-points, Space Group and First Brillion Zone	21
3.3.3 Electronic band structure	22
CHAPTER-FOUR	23
RESULT AND DISCUSSION	23
4.1 Hafnium Oxide Supercell	23
4.2 Geometry Optimization	23
4.3 Structural stability of hafnium oxide	25
4.3.1 Formation Energy	25
4.3.2 Cohesive Energy	25
4.4 Electronic Properties.....	26
4.4.1 Band structure and Density of States	26
4.5 Born Effective Charge	31
4.5.1 Calculated Born effective charge of pure HfO ₂	32
4.5.2 Born effective charge of silicon doped hafnium oxide.....	32
CHAPTER -FIVE	37
CONCLUSION AND RECOMMENDATIONS	37
5.1 Conclusion	37
5.2 Recommendations.....	38
APPENDICES	39
Appendix A.....	39
Appendix B	44
Appendix C	46
References.....	47

D. LIST OF FIGURES

Figure 1. 1 Schematic diagram of domain structure with domain boundaries [6].....	2
Figure 1. 2 Ferroelectric hysteresis loop with polarization states [2].	3
Figure 1. 3 Polymorphs of HfO ₂ are A) Monoclinic B) Orthorhombic C) Tetragonal D) cubic [7]	5
Figure 1. 4 (a) Parallel plate capacitor representation (b) Charge separation under an electric field [8].....	6
Figure 1. 5 Remnant Polarization versus Temperature [9].	8
Figure 1. 6 Switching Time versus Temperature [10].	8
Figure 2. 1 Typical hysteresis curve of a ferroelectric film. Ec is the coercive field [15].	15
Figure 4. 1 Geometry optimization of hafnium oxide a) Energy cut off optimization b) k- points optimizations.	24
Figure 4. 2 First Brillion zone and high symmetry points of hafnium oxide.....	27
Figure 4. 3 Calculated band structure of pure HfO ₂	27
Figure 4. 4 Calculated Band structure of Si doped HfO ₂	28
Figure 4. 5 Calculated TDOS of pure HfO ₂	29
Figure 4. 6 Calculated TDOS of Si doped HfO ₂	29
Figure 4. 7 Calculated partial density of (PDOS) pure HfO ₂	30
Figure 4. 8 Calculated partial density of Si doped HfO ₂	31

E. LIST OF ACRONYMS

Crystalline structure and densities.....	XCrysDen
Complementary metal oxide semiconductor.....	CMOS
Density functional theory.....	DFT
Density of State.....	DOS
Ferroelectric random access memory.....	FeRAM
Integrated circuit.....	IC
Generalized Gradient Approximation.....	GGA
High-angle annular dark-field scanning transmission electron microscopy	HAADF-STEM
Local density approximation.....	LDA
Lead zirconate titanate.....	PZT
Metal oxide semiconductor field-effect transistor.....	MOSFET
Perdew-Burke-Ernzerhof.....	PBE
Position averaged convergent beam electron diffraction.....	PACBED
Self-calculation field	SCF
Ultra soft pseudopotentials.....	USP
Visualization for Electronic Structural Analysis.....	VESTA

CHAPTER-ONE

INTRODUCTION

1.1 General background

As we all know, this is the age of information, and storage is one of the key issues. A computer system, whether a large machine or a microcomputer, requires memory for storing data and program instructions. Furthermore, within a given computer system, there are typically different types of memory that use different technologies and have different access times. Ferroelectric materials have attracted much attention for their practical use as capacitors in non-volatile memories. Ferroelectricity is a property of an insulating crystal or dielectric that shows spontaneous polarization, which must be switchable by the application of a suitable electric field. [1].

A ferroelectric has two or more distinct stable or metastable states of nonzero polarization. In all the known ferroelectrics, spontaneous polarization is developed by the atomic arrangements of the atoms inside the crystal [2]. Note that only a crystal with a polar space group can present a non-zero polarization. In ferroelectric materials, the electric dipoles are usually not uniformly aligned in the same direction throughout the entirety of the material. They are arranged in different directions in some order to minimize the free energy in the material [3]. The polar crystal structure can be obtained through symmetry-breaking from a high-symmetry nonpolar reference structure. Thus, we can calculate the magnitude of the polarization (P_s) using the born effective charges (Z) and the atomic displacements (u) from the reference state as follows in Eq. 1: Ω the volume of the unit cell. In most ferroelectrics, there is a phase transition from a high-symmetry Paraelectric phase to a low-symmetry ferroelectric phase with decreasing temperature.

$$P_s = \frac{1}{\Omega} \sum Z^* U \quad (1)$$

A domain is a region where all the elementary dipoles are aligned in the same direction. Domains are typically 10 nm to 1 μ m in size [4]. The boundary or interface between these domains have

spontaneous polarization oriented in a different direction as in Figure 1.1. Are known as domain walls. These walls are transition regions where the direction of spontaneous polarization from one direction gradually aligns with the spontaneous polarization of the adjacent domain. The distribution of the domain wall is dependent on the crystal structure of a ferroelectric unit cell. The tetragonal phase aligns the neighboring domains to be either perpendicular (90° orientation) or antiparallel (180° orientation) to each other, whereas the rhombohedral phase gives rise to 109° and 70° orientations. The domains are further subdivided into 1-10 μm regions known as grains with random orientations.

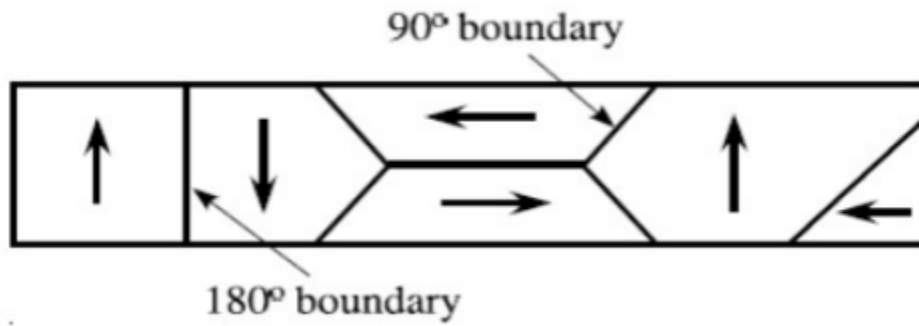


Figure 1. 1 Schematic diagram of domain structure with domain boundaries [6].

The interface between the grains is termed "grain boundaries," which can be visualized as a 2D relation. Further, the polycrystalline material may have defects and cracks. The macroscopic net polarization in the ferroelectric material is termed the "remnant polarization," which is typically less than the spontaneous polarization. The direction of polarization in a randomly oriented ferroelectric can be aligned in a particular direction by the application of a sufficiently strong electric field. The process is called poling [5]. When the electric field is increased in the same direction, the dipole moments are forced to align in the same direction as the electric field and form a ferroelectric domain state in single crystals, unless the applied electric field causes material failure. Once the material is poled, switching the orientation of the domains within the material induces a hysteresis loop, as seen in Figure 1.2. The remnant polarization (P_r) corresponds to the material's polarization without the applied electric field (E), and the saturation polarization (P_s) is

reached at the high field range. The switching field (E_{coerc}) is called the coercive field of the hysteresis loop [3-7]. The role of the coercive field is to measure the ability of ferroelectric material to withstand an external electric field without becoming depolarized.

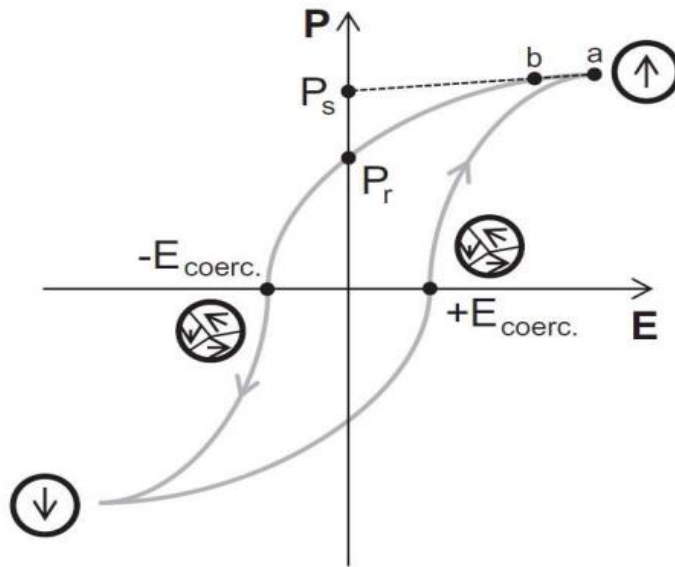


Figure 1. 2 Ferroelectric hysteresis loop with polarization states [2].

1.2 Hafnium Oxide Overview

HfO₂, representing a class of simple binary oxides, ferroelectric films based on hafnium oxide have received widespread attention due to their lead-free, simple binary oxide nature, excellent CMOS compatibility, and sub-10 nm scaling ability. Such excellent properties make this new type of ferroelectric material very promising for realizing low-power and high-density nonvolatile memories. Hafnium (HfO₂) is a technologically important compound that has been used as gate dielectrics, protective layers, optical coatings, and refractory materials due to its high dielectric constant, large band gap, and good reliability, compatibility with processing steps, high refractive index, high bulk modulus, and melting point.

Hafnium (IV) oxide is the inorganic compound with the formula HfO₂. Also known as hafnium dioxide or hafnia, this colorless solid is one of the most common and stable compounds

of hafnium. It is an electrical insulator with a band_gap of 5.3–5.7 eV. At room temperature and atmospheric pressure, HfO₂ in its bulk form exhibits the monoclinic P21/c (m-phase), which is the most stable phase. HfO₂ will change their phase from monoclinic to tetragonal P42/nmc (t-phase) and then to cubic Fm-3m when the temperature rises to 1700 °C and then 2600 °C (c-phase) [7].

When hydrostatic compressive pressure is applied to the m-phase of HfO₂, orthorhombic phases (o-phase), such as Pbcu at 4 GPa and Pnma at 14.5 GPa, begin to develop. Since all of the aforementioned HfO₂ polymorphs have inversion symmetry, any connection to ferroelectricity can be disregarded. Surprisingly, ferroelectricity was found in thin films of Si-doped HfO₂ that were 10 nm thick and contained less than 4% Si dopant. According to Boscke [3] the development of the polar orthorhombic phase Pca2₁ is what causes the ferroelectricity that was seen (Fig. 1.3). In Mg doped ZrO₂ ceramics, Kisi and Howard [4] used neutron powder diffraction to discover this o-phase for the first time. (Note: ZrO₂ and HfO₂ are structurally and chemically related.)

In later theoretical work Huan [5] revealed that both Pca2₁ and Pmn2₁ phases had low free energies and low energy barriers for polarization switching, they hypothesized that two orthorhombic phases with polar space groups of Pca2₁ and Pmn2₁ might represent the ferroelectric phases of HfO₂. More recently, Sang[6] used position averaged convergent beam electron diffraction in conjunction with high-angle annular dark-field scanning transmission electron microscopy (HAADF-STEM) to support their claim that the Pca2₁ phase is the structural source of ferroelectricity in Gd:HfO₂ thin films position averaged convergent beam electron diffraction (PACBED). There are many factors reported to be responsible for causing the anisotropic stresses and thus stabilizing the ferroelectric o-phase during the film growth, such as doping, surface energy effect, island coalescence, thermal expansion mismatch, capping layer effect, and the formation of oxygen vacancies.

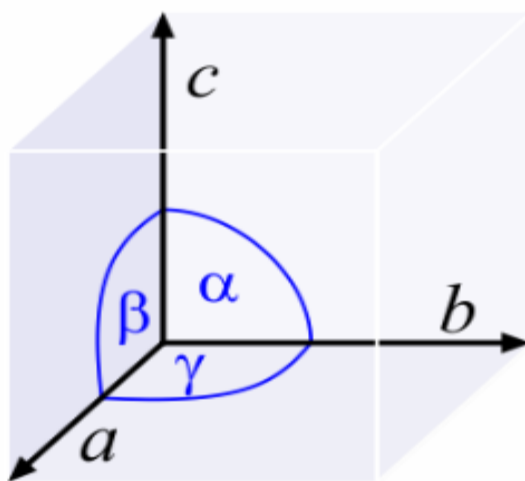
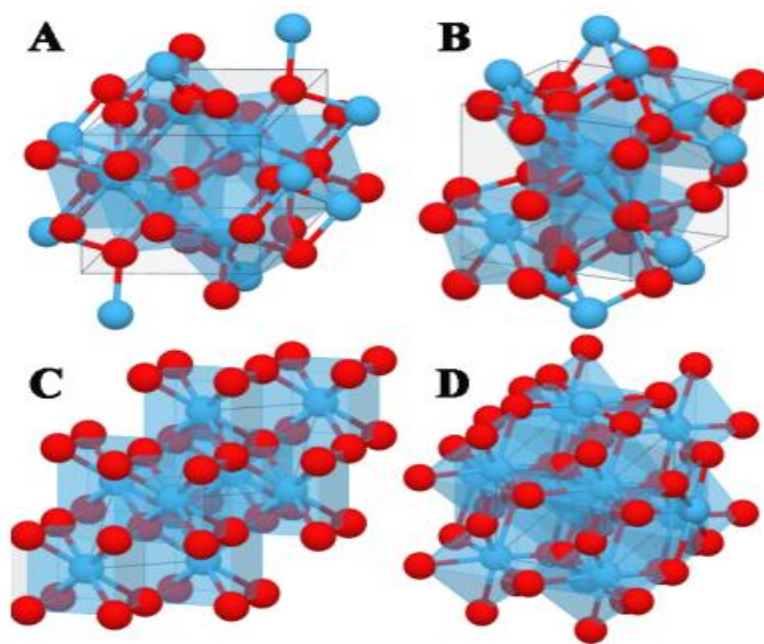


Figure 1.3 Polymorphs of HfO₂ are A) Monoclinic B) Orthorhombic C) Tetragonal D) cubic [7].

1.3 Dielectric properties and Energy storage

A capacitor consists of two parallel conducting plates of area A that are separated by a certain dielectric material with thickness d and subjected to an electric field, E , as seen in Figure 1.4. The dielectric constant, or relative dielectric permittivity, is a material property that determines the degree of electric polarization in response to the applied electric field [13] and is represented as the ratio of its absolute permittivity to the electric constant as in Eq. 2 and 3. The electric field, E , is represented by Gauss' law, where Q is the charge density and ϵ_0 is the permittivity of free space, which is approximately 8.851012 F/m .

$$E = Q/\epsilon_0 \quad (2)$$

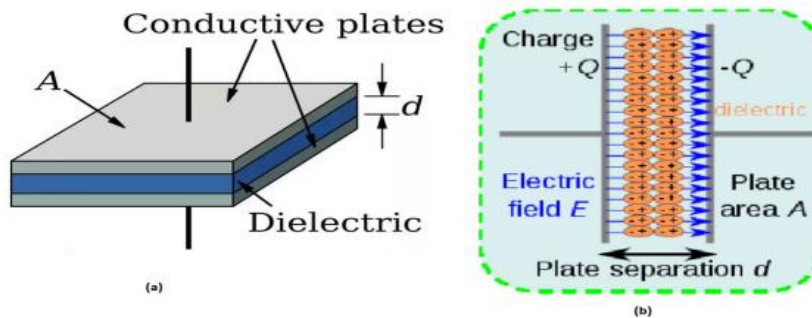


Figure 1. 4 (a) Parallel plate capacitor representation (b) Charge separation under an electric field [8].

$$\epsilon_r = \epsilon/\epsilon_0 \quad (3)$$

Under any given voltage (V) a capacitor can store electric charge (Q) as in Eq. 4

$$Q = CV \quad (4)$$

Here C is the capacitance of the capacitor, which is a measure of charge per electric potential (1 Coulomb/1 Volt = 1 Farad (F)) and is given by the expression in Eq. 5. In that equation, ϵ and A are the

relative permittivity of the dielectric and permittivity of free space, "A" is the area of the conducting plate, and "d" is the thickness of the dielectric between the conducting plates. Hence, the capacitance of the capacitor can be increased by increasing the area and decreasing the thickness or by increasing the permittivity of the dielectric medium.

$$C = \epsilon_r \epsilon_0 \frac{A}{d} \quad (5)$$

When the area of the conducting plate is increased and the separation distance between plates is decreased, we use dielectric material between them, which has a higher dielectric breakdown strength. Also, capacitance has a direct relationship with the area and an indirect relationship with the distance between two plates.

1.4 Environmental Influences on Ferroelectric Materials

1.4.1 Temperature

Temperature affects the characteristics of ferroelectric materials. This includes the remnant polarization of the material, one of the critical parameters for memory applications, which decreases as temperature increases until the Curie temperature is reached. The reduction is relatively gradual at lower temperatures but becomes more dramatic as the Curie temperature is approached, at which point the material enters the Paraelectric phase and the material loses its capability to switch polarization and retain a set state [15]. For memory applications, this temperature dependence must be considered in the design process when establishing the required minimum levels of initial remnant polarization. This dependence on temperature also limits the

materials useful for memory applications to those with Curie temperatures significantly above the maximum military specification of 125 °C.

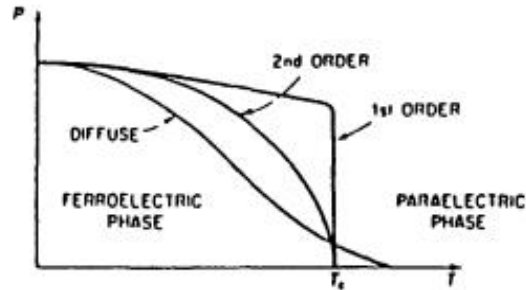


Figure 1. 5 Remnant Polarization versus Temperature [9].

Switching time is also a function of temperature. As temperature increases toward T_c , the switching speed of the material increases. As the temperature rises to T_c , switching time extrapolates to zero [16]. Figure 1.6 shows this relationship for ferroelectric thin films.

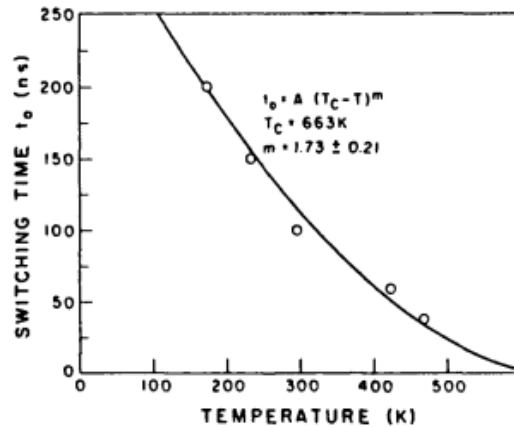


Figure 1. 6 Switching Time versus Temperature [10].

1.4.2 Grain Size

Coercive field, Curie temperature, remnant polarization, aging rate, and fatigue resistance are all variables that the ferroelectric material's grain size can have a significant impact on. While remnant polarization is directly proportional to grain size, the coercive field, aging rate, fatigue rate, and Curie temperature are inversely related [19]. These effects appear to be the product of an internal space charge field [12] that forms within the material domains and protects them from the external electric field. It has also been shown that the polarization switching time increases with decreasing particle size. Given that each deposition technique generates a typical range of grain sizes, these correlations between the key ferroelectric characteristics and grain size may be crucial when deciding which of the various deposition procedures to use. The performance of the produced thin film is the primary performance criterion when weighing the benefits and drawbacks of each process [13].

1.5 Statement of the problem

Despite more than 60 years of intensive research, FeRAM has only been used in a small portion of the memory market. The reason for this is that the most advanced FeRAM is based on perovskite ferroelectrics, including Pb (Zr, Ti) O₃ (PZT) and SrBi₂Ta₂O₉ (SBT) [20], which have problems like poor complementary metal-oxide semiconductor performance (CMOS) compatibility and limited scalability. The integration of perovskite ferroelectrics and related electrodes into the CMOS platform is complicated by the CMOS compatibility issue, which increases manufacturing and processing costs. Meanwhile, the scaling problem restricts the memory cell's size, which results in a poor memory density.

Therefore, finding solutions to these problems is crucial for the continued development of FeRAM. The first finding of ferroelectricity in ultrathin Si-doped HfO₂ films in 2011 [21] has opened up possibilities for resolving the aforementioned problems with ordinary perovskites. HfO₂, which belongs to a group of straightforward binary oxides, is already widely used in CMOS technology as a high-k dielectric material.

Ferroelectric materials contain bi-stable polarization states Pr, which can be used to non-volatilize and store binary information of 0 and 1. An electric field drives the transition between polarization states 0 and 1 (i.e., two polarization states), which results in extremely little energy loss. Due to this significant advantage, ferroelectric random access memory (FeRAM) is very competitive with other new current-driven nonvolatile memory technologies, including phase-change RAM and resistive RAM (RRAM). Various dopants, such as Si, Al, Y, Gd, La, and Sr, are used to calculate the different properties of hafnium oxide and improve the ferroelectricity. There is a band shift after doping different elements in HfO₂ [22]. Also, born effective charge properties were studied before this, and they show the magnitudes of the born effective charges of the Zr and oxygen atoms are greater than their nominal ionic valences (+4 for Zr and -2 for oxygen), indicating a strong dynamic charge transfer from Zr atoms to O atoms. This effective charge transfer shows there is good remnant polarization in our material, and it is possible to replace perovskite material with modern hafnium oxide material.

1.6 Objectives of the research

1.6.1 General objective

- The general objective of this study was to investigate the effect of silicon doping on the structural, electronic, and born effective charge properties of monoclinic hafnium oxide using density functional theory.

1.6.2 Specific objectives

The following were the study's specific objectives:

- To optimize parameters such as energy cutoff and k-points.
- To calculate the formation energy for doped hafnium oxide.
- To calculate the band structure and DOS of pure hafnium oxide.
- To calculate the cohesive energy, DOS, and band structure of the silicon-doped hafnium oxide,
- To calculate born effective charge of pure and silicon doped hafnium oxide.

1.7 Significance of the study

The significance of this study would help to understand the electronic, structural, and born-effective charge properties of pure and silicon-doped monoclinic hafnium oxide using a computational technique known as DFT. The significance of studying structural properties is that structures determine the arrangement of atoms in a particular material. It also denotes the bond lengths and lattice parameter of a specific material. The atomic arrangement is responsible for the strength and ductility of the material. The significance of studying electronic properties is that it provides an understanding of the behavior of electrons within materials, how electrons determine the optical and electrical properties of materials, and how electronic properties are controlled for use in non-volatile memory technological applications. The significance of studying the born-effective charge properties is to know the electrical polarization induced by the displacement of individual atomic sub lattices.

1.8 Scope of the study

The main focus of this thesis is the investigation of the effects of silicon doping on ferroelectrics based on monoclinic HfO_2 . The structural stability and cohesive energy of the structure were calculated. Born-effective charges were calculated using first-principles calculations based on density functional theory (DFT). This work is limited to studying the theoretical properties and increasing silicon-doped HfO_2 systems by simulating at the atomistic and electronic scales, which doesn't involve any experimental work.

CHAPTER -TWO

LITERATURE REVIEW

2.1 Overview of Ferroelectric Materials

Ferroelectricity has been widely studied for years and achieved in various materials. Nonvolatile memory devices fabricated using ferroelectric materials are based on polarization switching, which is stable and can be operated at high speeds. Since SiO₂'s development as a gate dielectric material decades ago, it has served as the cornerstone of the current integrated-circuit (IC) industry. Driven by the seemingly endless pressure for higher operation speed, smaller physical dimensions, and lower driving voltage, the gate dielectric thickness in the IC [23] industry has been rapidly reduced from the order of 12 m in the early 1960s to the current value of about 23 nm. If SiO₂ is not replaced by another dielectric material, this would require the gate-dielectric thickness to be reduced to less than 1 nm [24].

A reduction in gate SiO₂ thickness would impose several severe problems on the current SiO₂ semiconductor technology, including a high level of direct tunneling current and reliability problems associated with the non-uniformity of the very thin SiO₂ film.

The current solution to overcome this problem is being proposed. Candidates include ZrO₂, HfO₂, Y₂O₃, Al₂O₃, Ta₂O₅, etc. HfO₂ is the most common high-gate dielectric among these candidates, and it is used in cutting-edge metal-oxide semiconductor field-effect transistors (MOSFETs) [25]. Hafnium oxide (HfO₂) is an important candidate for SiO₂ replacement as a gate material due to its high dielectric constant of 25 at 300 K, which is about six times higher than that of SiO₂. The technological importance of HfO₂ increases if we consider its high bulk modulus and melting point (27000 °C). At normal temperature and pressure its structural phase is monoclinic (space group P21/c) at 1700°C.

The overall properties of ferroelectric materials are improved by doping different elements such as Ca, Gd, La, Al, Ce, and other elements. Among this lanthanide series of elements, the dopants

have the strongest effect on the stabilization of the ferroelectric phase in hafnium oxide. The electronic properties of ZnO and Ba-doped ZnO materials were evaluated through the projected densities of states (DOS) and TDOS. After doping Ba to ZnO, the band structure shifted, and after doping, the value of the band gap was also decreased [26]. The electronic properties of BaTiO₃ doped with La show the electronic band structure has shifted towards the conduction band, and its value is 1.569 eV. Calculations show that the nature of the band structure in doped material has shifted from indirect (pure) to direct. The minimum energy required for excitation of an electron is determined by the band gap in insulators and semiconductors, but it cannot completely describe whether a phonon will be absorbed by the material or not. The shift in the band gap in BaTiO₃ after La doping indicates an increase in material conductivity due to readily occurring hole-electron recombination in the direct band gap [27].

The other property is born effective charge; in ZrO₂, the magnitudes of the born effective charges of the Zr and oxygen atoms are greater than their nominal ionic valences (+4 for Zr and -2 for oxygen), indicating a strong dynamic charge transfer from Zr atoms to O atoms.

2.2 Conceptual Framework

The theoretical capacity of FeRAM, made of hafnium oxide, has recently been increased by a variety of processes, including doping with rare earth elements like La (lanthanum), Gd (gadolinium), Ce (cerium), and Sr (strontium). With regard to typical ferroelectrics like lead titanate zirconate, ferroelectric HfO₂ has a coercive field, scalability of layer thickness, and other advantages. This has allowed for highly scalable devices in 28, 22, and 14 nm (PZT) technology [28].

The dopants with the biggest impact on stabilizing the ferroelectric non-centrosymmetric orthorhombic phase in hafnium oxide are those from the lanthanide series. This finding was confirmed by adding La and Gd to HfO₂, which show the highest remnant polarization values of all hafnia-based ferroelectric films until now [29]. After doping lanthanide elements into ferroelectric material, the band structure has shifted to a conduction band.

2.3 DFT Study of Hafnium Oxide

DFT has increasingly been utilized in recent years to model the behaviors of energy storage materials and to explain how they work. When anticipating the characterization and modeling of novel materials, DFT is incredibly accurate. GGA functional, particularly the Perdew-Burke-Ernzerhof (PBE) GGA, are the main functional used in hafnium oxide memory. It is used to compute the born effective charge, electronic properties, optical, vibrational, and polarization. DFT simulations demonstrate benefits for investigating reaction processes at the atomic scale and for virtually screening new ferroelectric materials to lower the development cost as compared to experiments [30].

DFT can be used to either distinguish between the possibilities that were left open or to explain the assumptions that have been drawn from the analysis of the trials. A strong relationship between theory and observation is enabled by the calculation of a wide range of molecular properties using DFT, and this frequently yields important hints regarding the geometric, electronic, and spectroscopic characteristics of the structures under investigation [31].

2.4 Application of HfO₂ Ferroelectric material

Thin-film hafnium oxide can be used for non-volatile memory devices. The two-level logic needed for these devices relies on the two remnant polarization states, their non-volatility, and the constant remnant polarization even at zero field. However, ferroelectrics (HfO₂) can also be used in other applications, such as micromechanics (actuators and MEMS) and electro-optics, since their refractive index changes with the voltage applied. These applications rely heavily on ferroelectrics' ability to be pyro- and piezoelectric.

Furthermore, ferroelectrics can also be used for cooling and electron emission [33]. New types of memories called ferroelectric memories (FeRAMs) use electrical polarization to store information rather than the electrical charge used in traditional memories. Due to their non-volatility, high integration scale due to small DRAM-like cell sizes, fast read and write speeds, and low

Voltage /low power characteristics, FeRAMs are appropriate for memory and mobile applications. FeRAMs make use of the electrical polarization's hysteresis behavior in relation to the electric field. Figure 2.1 illustrates that there are two remnant polarization states ($+P_r$ and $-P_r$) at zero field that can be used to store the logical values "0" and "1." These polarization states can change from one to another by applying an electric field that is sufficiently strong ($E > E_c$, where E_c is the coercive electrical field) [34].

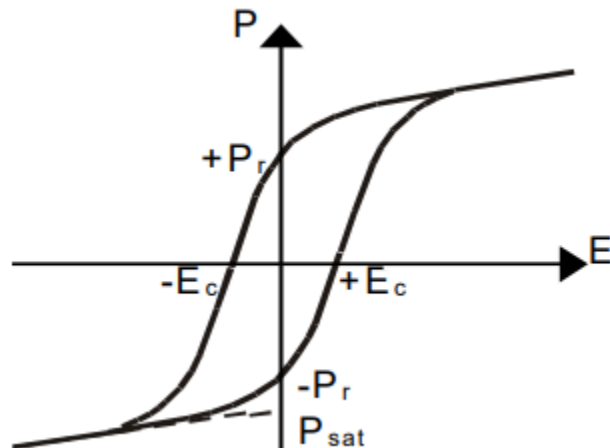


Figure 2. 1 Typical hysteresis curve of a ferroelectric film. E_c is the coercive field [15].

CHAPTER -THREE

METHODOLOGY

3.1 Methods

The study was purely theoretical. The main sources of information are published articles, books, theses, and dissertations. Software and computers are additional instruments used to accomplish this project.

3.2 Computational methodology

The overall calculations in this work were performed under various categories. The first energy cutoff and k points (billion zone sampling) are optimized. The cell was then relaxed to obtain the system's minimum energy before performing the other calculation. Hafnium oxide is a ferroelectric material with many polymorphs such as monoclinic, tetragonal, orthorhombic, and cubic crystal structures, of which we have chosen the monoclinic crystal structure for our research where $a = b \neq c$ and $\alpha = \gamma = 90^\circ$, $\beta \neq 90^\circ$) and space group of $P2_1/c$ and It has 12 atom per unit cell. The lattice parameter of monoclinic HfO_2 used in this work is ($a=5.14\text{\AA}$, $b=5.19\text{\AA}$, $c=5.32\text{\AA}$) [26]. The reason for selecting a monoclinic crystal structure is that it is easily stable at room temperature and pressure, and we can easily obtain the lattice parameter from the article, whereas the lattice parameter of other crystal structures is not the same for others; as a result, it is suitable for calculation, and it exhibits ferroelectric behavior up to Curie temperature.

We used $5 \times 5 \times 5$ for both doped and pristine hafnium oxide. For doped hafnium oxide, one silicon atom is substituted by one Hf atom, which corresponds to 4.166%. The band structures of pristine and Si-doped hafnium oxide were calculated by using $5 \times 5 \times 5$. For DOS, a dense k-point of $18 \times 18 \times 18$ was used.

During the optimization of the cut-off energy, the k-points were kept constant at $5 \times 5 \times 5$, and the lattice constant was taken from the literature and agreed with the experimental value. After

minimum energy were reached, the optimum value of cut off energy was taken. Then, to optimize k- points, we use the experimental value of lattice constant while keeping cut off energy at (35Ry) 478eV. Finally, by using the experimental value of lattice constant from literature cut off energy and k-point was optimized.

Our calculations are based on Density Functional Theory (DFT) with the Perdew-Burke-Ernzerhof (PBE) exchange-correlation functional, Vanderbilt ultra-soft pseudopotentials [36], and the plane wave basis set implemented in the Quantum Espresso program package [37]. Quantum ESPRESSO is an integrated suite of computer codes for electronic-structure calculations and materials modeling based on density-functional theory (DFT), plane wave basis sets (PW), and pseudo potentials (PP) [38].

It is freely available and distributed as open-source software under the terms of the GNU General Public License (GPL). The present applicability of quantum ESPRESSO ranges from simple electronic structure calculations to the most sophisticated theoretical spectroscopy such as nuclear magnetic resonance (NMR), electron paramagnetic resonance (EPR), Raman, scanning tunneling microscopy, etc.

The simulation tools implemented in Quantum ESPRESSO are used across a wide range of R and D applications. The relevance of this code has been highlighted by its adoption in a number of key research groups and renowned institutions, as well as in a number of commercial industries. The most important input parameters in Quantum Espresso are the atomic geometries (number and types of atoms in the periodic cell, Bravais-lattice index, crystallographic or lattice constants), the kinetic energy cutoff, and the type of pseudopotentials [40].

The formation energy of doped hafnium oxide was calculated as follow:

$$E_{form} = E_{HfO_2, Si(crystal)} - E_{Hf(crystal)} - E_{O_2(crystal)} - E_{Si(crystal)} \quad (6)$$

where $E_{HfO_2, Si}$, E_{Hf} , E_{O_2} and E_{Si} are the total energies of HfO_2, Si , Hf , Si and O at their most stable states, respectively.

In this work, cohesive energy (E_{coh}) is also estimated to verify the material's structural stability. The combined energy provided by the unbound atoms in a crystal is known as cohesive energy. The bonding force between the atoms in a crystal increases with the cohesive energy's absolute value, making the crystal more stable as it forms.

The formula calculating for cohesive energy as follow:

$$E_{co} = \frac{m \times E(\text{Hf}) + n \times E(\text{O}_2) - E(\text{HfO}_2)}{m + n} \quad (7)$$

Where HfO_2 denotes a compound; m and n denote the number of Hf and O in the formula (HfO_2), $E(\text{Hf})$ and $E(\text{O})$ denote the energies of compound HfO_n , isolated atom A , and isolated atom B , respectively and E_{CO} is the cohesive energy. When the cohesive energy of the structure is higher, it is significantly more stable. VESTA and XCrystDen used for visualization of the structure.

3.3 Electronic structure calculation

The structure of atoms, crystals, molecules, surfaces and their interactions are computed by Density Functional Theory (DFT) [41]. It relies on Hohenberg and Kohn and Sham approximation that can follow the local density approximation (LDA) or the generalized gradient approximation (GGA) to generate accurate results, for various structural and energetic properties of bulk materials and surfaces, interfaces and point defects. Physical properties of molecules take their origin in electron assembly phenomena. To understand these properties, one must investigate electron distributions and interactions which is contained in the electronic wave function governed by Schrödinger's equation:

$$\hat{H}\Psi = E\Psi \quad (8)$$

Which is defining the N-electron Eigenfunction Ψ and eigenvalue E of the Hamiltonian \hat{H} . Hamiltonian \hat{H} is given by,

$$\hat{H} = \frac{p^2}{2m} + V(r) \quad (9)$$

for single electron Not all values for the energy are allowed and one calls the allowed values eigenvalues. The functions Ψ which belong to the eigenvalues, and which are a solution of the vibration equation and, in addition, satisfy the boundary conditions, are called eigenfunctions of the differential equation. The non-relativistic Hamiltonian is written as the sum of different kinetic and potential contributing arising from interacting electrons and nuclei:

$$\hat{H} = T_N + T_e + V_{Ne} + V_{ee} + V_{NN} \quad (10)$$

Where T_N , T_e , V_{ee} and V_{NN} are kinetic energy of nuclei, the kinetic energy of an electron, interaction potential between nuclei and electrons, interaction potential between electrons and electrons, and interaction potential between nuclei and nuclei.

According to the Born-Oppenheimer approximation (BOA) the nuclei are considered immobile due to their masses are much heavier than the electrons and their kinetic energy is much lower, and the problem is solved by considering only the electronic part of the Hamiltonian. Thus, the electronic Hamiltonian using atomic units given as:

$$\hat{H}_{elec} = \sum_i \left(-\frac{1}{2} \Delta_i\right) - \sum \sum_A \frac{Z_A}{r_{iA}} + \frac{1}{2} \sum \sum \frac{1}{r_{ij}} \quad (11)$$

While the first two terms are mono-electronic in nature, the third one is the electron-electron repulsion which excludes any analytical resolution of the many-body problem. Generally, DFT calculations allow investigating the electronic structure of nanomaterials and thus predicting their fundamental properties, help their characterization, justify the experimental results, and forecast the potential application.

The main equation of DFT was explained by Kohn-Sham. In this case there are two theorems which postulate the properties of any system. The first theorem explains as the ground state energy is the unique function of electron density i.e., $E_0 = E(n_o(r))$ while the second theorem describes the electron density that minimize the energy of the system is true ground electron density. Based on these theorems if someone get the electron density of the system it is easily to calculate the ground energy and know all properties of the system at ground states. The overall Kohn-sham equation is given as

$$\left[-\frac{1}{2}\nabla^2 + V_{ext}(\mathbf{r}) + V_H(\mathbf{r}) + V_{xc}(\mathbf{r})\right]\varphi_i(\mathbf{r}) = E\varphi_i(\mathbf{r}) \quad (12)$$

Where V_{xc} is exchange correlation potentials which make difference from the previous formula.

3.3.1 Exchange-correlation energy

The KS DFT provides a practical procedure to solve the many-body problem by breaking the problem into a set of single-particle problems. This formalism is exact but practically still unsolvable since the many-body wave functions are still included in the exchange-correlation term $E_{xc}[n]$, whose exact form is not known.

To make the formalism useful, it is necessary to make some approximations for the exchange-correlation term $E_{xc}[n]$. The most common and straightforward approximation to $E_{xc}[n]$ is the Local Density Approximation (LDA). The idea of the LDA [42] is assuming that the exchange-correlation energy per electron of a non-uniform system at any point in space is equal to the exchange-correlation energy per electron in a uniform electron gas having the same density at this point. In LDA the exchange-correlation functional can be written as

$$E_{xc}^{LDA}[n] = \int d\vec{r} \mathcal{E}_{xc}[n]n(\vec{r}) \quad (13)$$

With

$$\mathcal{E}_{xc}[n] = \mathcal{E}_{xc}^{uniform}[n] \quad (14)$$

By definition, the LDA is local because the exchange correlation energy $\mathcal{E}_{xc}[n]$ at each point in space only depends on the electron density at the same point. The $\mathcal{E}_{xc}[n]$ has been calculated and parameterized through Monte Carlo total energy calculation for a uniform electron gas with a variety of electron densities [43].

Since the LDA is based on uniform electron gas, it is expected to be accurate only for systems in which the electron density varies slowly. It is clearly not suitable for the situations where the electron density undergoes rapid changes, as in the case of covalent bounded solids. To overcome this deficiency of the LDA, another form of exchanged-correlation functional has been developed,

that is the Generalized Gradient Approximation (GGA) [44]. The GGA functional depends on the local electron density as well as the spatial variation of the electron density that is represented by the density gradient. The GGA functional can be written as

$$E_{XC}^{GGA}[n] = \int \mathcal{E}_{xc}[n] F_{xc}[n, \vec{\nabla}n] n(r) \overline{d\vec{r}} \quad (15)$$

The $E_{XC}^{GGA}[n]$ is the exchange correlation energy per particle of an electron gas and F_{xc} is a functional of the electron density and its gradient. The GGA method gives better total energies, especially for small molecules, but computationally it is more time consuming than LDA [45]. Generally, GGA has the following advantages over LDA.

- GGA improves ground state properties for light atoms, molecules and clusters.
- GGA predicts the correct magnetic properties of 3d transition metals such as body centered iron.
- Though GGA seems to be superior compared to LDA, it has several drawbacks. A GGA method fails to accurately treat the hydrogen bond. This defect is clearly manifested through expansion and hence softening of bonds [46].

3.3.2 K-points, Space Group and First Brillouin Zone

K-point grid is sampling point in Brillouin zone which rises from Bloch theorem. For our calculation the K-points file is used to specify the Bloch vectors (k-points) to sampling the Brillouin zone. There is different mechanism that can specify the k-point grids in the K-POINTS file. These could be through automatically producing regular mesh of points, through the beginning and endpoints of line segments, or as the clear list of points and weights. The actual values of the k-points will be optimized by quantum espresso code in SCF calculation, and the optimized values will use for other calculation purposes. Space groups are commonly used to classify the symmetry of crystalline structure which incorporate 32 type of point group symmetry on the arrangement of atoms within the unit cell and 14 types of Bravais lattices of unit cells. There are 230 types of space groups. Within the unit cell, Wyckoff positions are defined to describe the site symmetry group which are conjugate subgroups of space group [46,47].

3.3.3 Electronic band structure

In a solid-state physics, the electronic band structure gives the information about a range of energy levels an electron inside the solid can take up, and the band gap is closely related to the electronic conductivity.

The band gap of a material is directly related to its conductivity, and the electronic resistance of electrode materials could be analyzed using Density of State (DOS) plots. The DOS is essentially several different states at a certain energy level that electrons are permitted to occupy, that is, the number of electron states per unit volume per unit energy [48]. The physical properties such as optical absorption, electrical resistivity and electrical conductivities are successfully described by Band theory.

CHAPTER-FOUR

RESULT AND DISCUSSION

4.1 Hafnium Oxide Supercell

The system was modeled as $2 \times 1 \times 1$ hafnium oxide supercell with 24 atoms. one hafnium atom replaced by silicon atom which correspond to 4.166 % (atom percent).

4.2 Geometry Optimization

In this work, one hafnium atom is substituted by one silicon atom which corresponds to 4.166% of silicon. Most theoretical investigations begin with optimizing the geometry of the species under examination. The results of optimized cut off energy and k points are shown in figure 4.1

Pristine hafnium oxide consisting of 12 atoms were fully relaxed in xyz direction. For $2 \times 1 \times 1$ supercell, the lattice parameters increased to $a=10.2846 \text{ \AA}$ $b=5.1951 \text{ \AA}$ $c=5.2502 \text{ \AA}$. In case of pristine hafnium oxide, the optimized Hf-O bond length was 2.04 \AA which is almost close to the experimental value 2.15 \AA [49]. The optimized energy cutoff vs energy of pristine hafnium oxide and k points is shown in figure 4.1. After optimization the energy cutoff is converged at about 478 eV. The Hf-O bond around the doped atom is either stretched or compressed. It is in the range of 2.10 \AA to 2.13 \AA . The bond length of Si-O is around 1.67 \AA which is almost similar to previous computational work. The Si-O bond length decreases because of the small atomic radius of Si with respect to Hf.

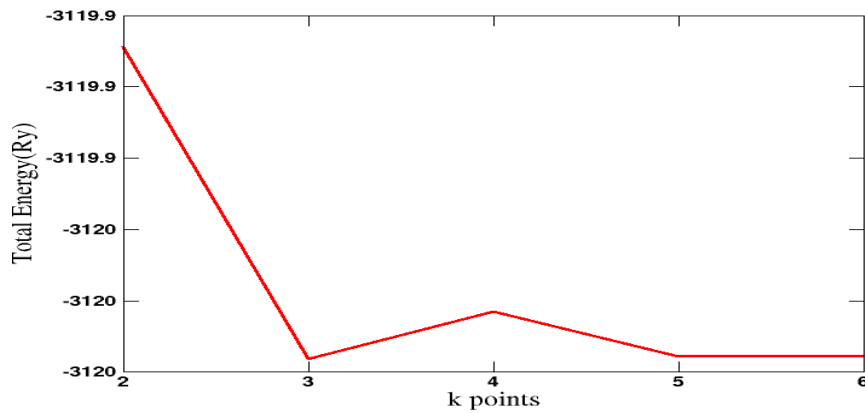
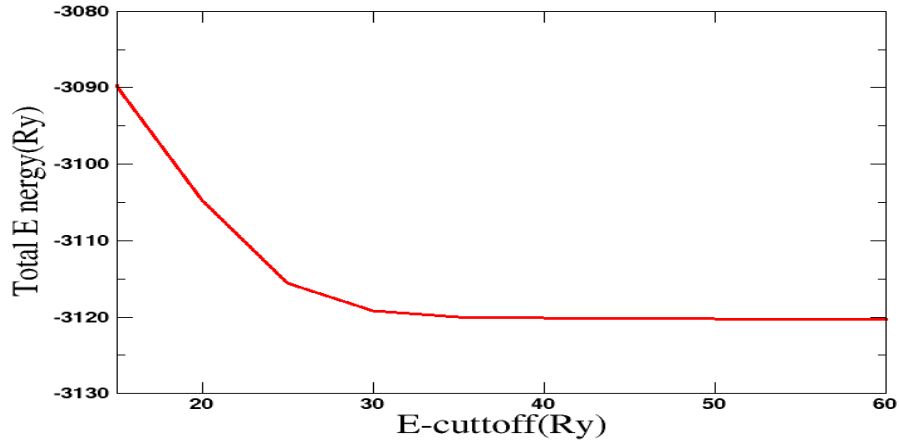


Figure 4. 1 Geometry optimization of hafnium oxide a) Energy cut off optimization b) k- points optimizations.

After 35 Ry and 5 X 5 X 5 in k point our material show linear graph because when the cut off also k point increase the total minimum energy already attained this is the reason why the graph linear.

4.3 Structural stability of hafnium oxide

4.3.1 Formation Energy

To examine the relative stability of Si atoms in pristine HfO₂, we have calculated the formation energy (E_{form}) using the following equation [50]:

$$E_{form} = E_{HfO_2, Si} - E_{Hf(crystal)} - E_{O_2(crystal)} - E_{Si(crystal)} \quad (16)$$

Where $E_{HfO_2, Si}$, E_{Hf} , E_{O_2} and E_{Si} are the total energies of HfO₂, Si, Hf, Si and O at their most stable states, respectively. The formation energy of each phase is negative, which indicates that all phases before and after doping can form stably in the system. The absolute value of formation energy of Hf is largest which indicates that it is the easiest to form in the system. Hence, Si atoms tend to preferentially replace Hf atoms in the HfO₂ lattice. The calculated formation energy is -8eV/atom it is good agreement with other work [51].

4.3.2 Cohesive Energy

Cohesive energy is used to predict the stability of the structure. The cohesive energy of pure hafnium oxide is given by the equation below.

$$E_{co} = \frac{m \times E(Hf) + n \times E(O_2) - E(HfO_2)}{m+n} \quad (17)$$

The calculated cohesive energy of pure hafnium oxide was -45 eV/atom and it is consistent with other previously calculated value [52].

For Si doped hafnium oxide:

$$E_{coh} = \frac{E_{HfO_2, Si} - (nE_{HfO_2} + mE_{Si})}{n+m} \quad (18)$$

Where $E_{HfO_2, Si}$, are total energy of Si doped hafnium oxide, n and m are number of atoms. The calculated cohesive energy for Si doped hafnium oxide was -46.32 eV/atom. The negative sign of cohesive energy indicates that the system is stable.

4.4 Electronic Properties

In this part, we aim to look into how Si doping affects the band structure and density of hafnium oxide. Using 5 X 5 X 5 K-points, band structure is calculated. A thick 18 X 18 X 18-point grid is also utilized for DOS.

4.4.1 Band structure and Density of States

Exploration of the band structure is a necessary prerequisite for investigating the systems' electronic properties. The electronic levels of a crystal structure are shown by the band structure. In terms of the band structure, many essential characteristics of crystals are explained.

By using first-principles calculations, the electronic structure of silicon-doped hafnium oxide and pristine hafnium oxide was determined. The energy band structures for pure and single-Si-doped 5 X 5 X 5 hafnium oxide supercells were plotted in order to comprehend the characteristics of the bandgap as well as the impact of Si-doping on the energy band structure. The band structure of hafnium oxide was calculated along the following path at the first Brillouin zone: Γ (0, 0, 0), R (0.5, 0.5, 0.5), S (0.5, 0.5, 0), X (0.5, 0), and Γ (0, 0, 0).

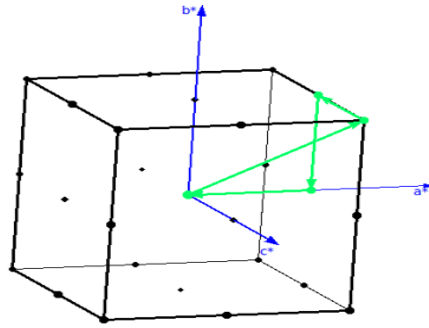


Figure 4. 2 First Brillouin zone and high symmetry points of hafnium oxide

The plots of band structures for HfO₂ at their respective ground state geometries are shown in Fig. 4.3. For all the structures, the Fermi level is set to zero energy. The band structure of HfO₂ shows an indirect bandgap, where the conduction band minima (CBM) and valence band maxima (VBM) are located at G and X, respectively. The magnitude of the gap is found to be 4.92 eV, which is in good agreement with the previously reported theoretical bandgap of 4.63 eV [53, 54] and less than the previously reported experimental band gap of 5.7 eV [55]. This is due to the known limitations of DFT calculations of GGA, which overestimate the lattice parameter and underestimate the band gap.

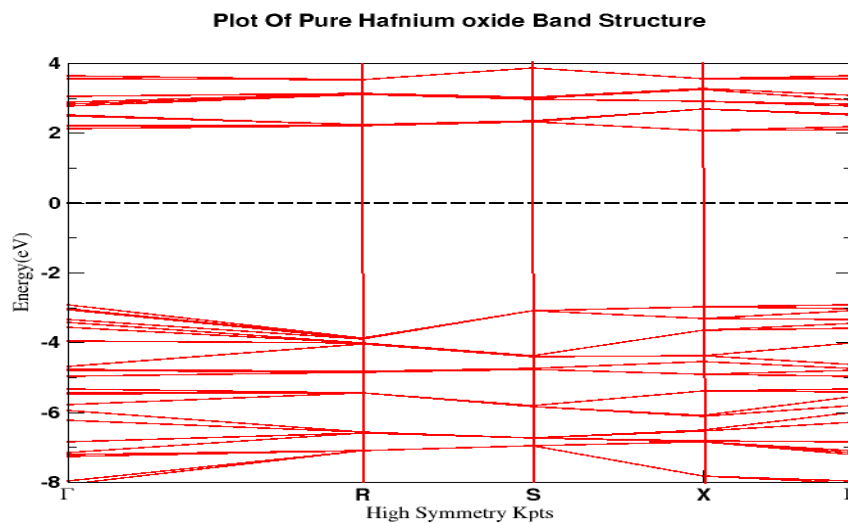


Figure 4. 3 Calculated band structure of pure HfO₂.

On the other hand, in Si-doped hafnium oxide, the Fermi energy moves up to CBM, which suggests that in the Si-doped system, the carriers are more likely to be electrons (N-type of conductivity). The magnitude of the gap was found to be 4.22 eV.

Because there is lattice distortion when we dope silicon, the band gap decreases after doping. The band structure seems straight because it is a problem of the quantum ESPRESSO software. When we use other software like VASP, the structure is not like this.

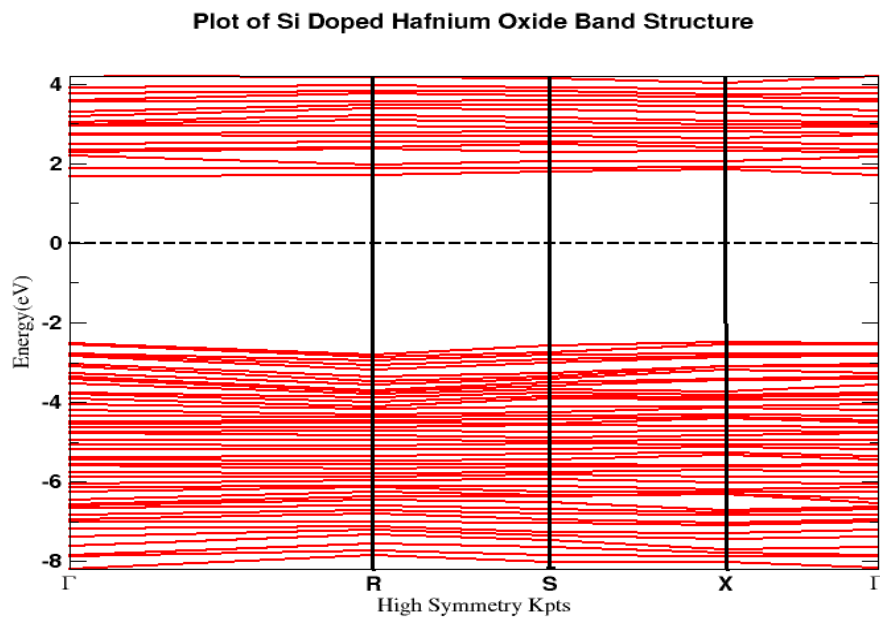


Figure 4. 4 Calculated Band structure of Si doped HfO₂

Another crucial factor in the examination of electronic property is the density of states (DOS). At a given energy level, the DOS represents the number of unoccupied states that an electron can occupy. Total and partial DOS charts can be used to show the contribution of various atoms.

HfO₂ is composed of three main bands: the lower valence band, the valence band just below the Fermi level, and the conduction band above 4.92 eV. The lower valence band is composed of mainly O 2s orbitals, while the valence band near Fermi level is essentially controlled by O 2p states with a minor presence of Hf-5d states. The presence of Hf 4p and 4s states in the valence

band range is negligible. The conduction band is composed essentially of Hf-5d states, separated from the valence band by an energy gap of 4.92 eV.

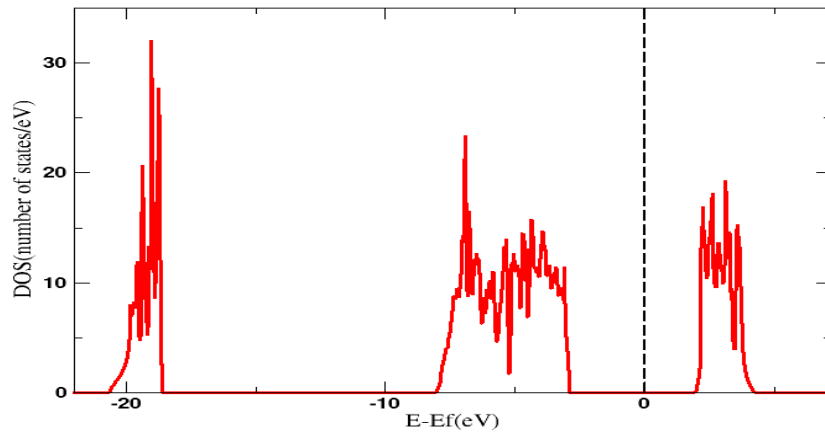


Figure 4. 5 Calculated TDOS of pure HfO₂

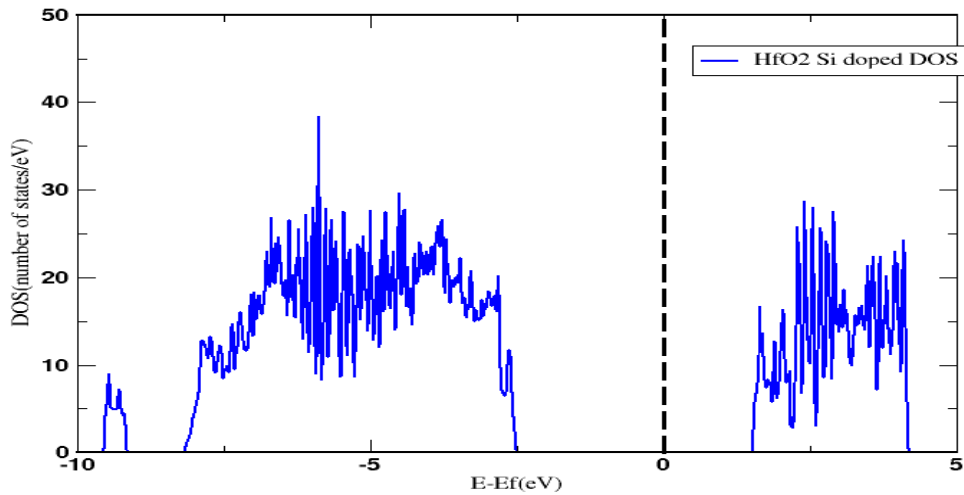


Figure 4. 6 Calculated TDOS of Si doped HfO₂

In addition, to determine which orbital contributes the most to the electronic properties, the partial density of states (PDOS) for pure and single Si-doped HfO₂ were plotted. As shown in Figure 4.7,

the hafnium d orbital and the oxygen p orbital make significant contributions to the state near the Fermi level drive.

However, for a single Si-doped hafnium oxide, the main contribution in the vicinity of the Fermi level is derived from oxygen P orbital electrons next to oxygen Si S orbitals also contributing, as shown in Figure 4.8.

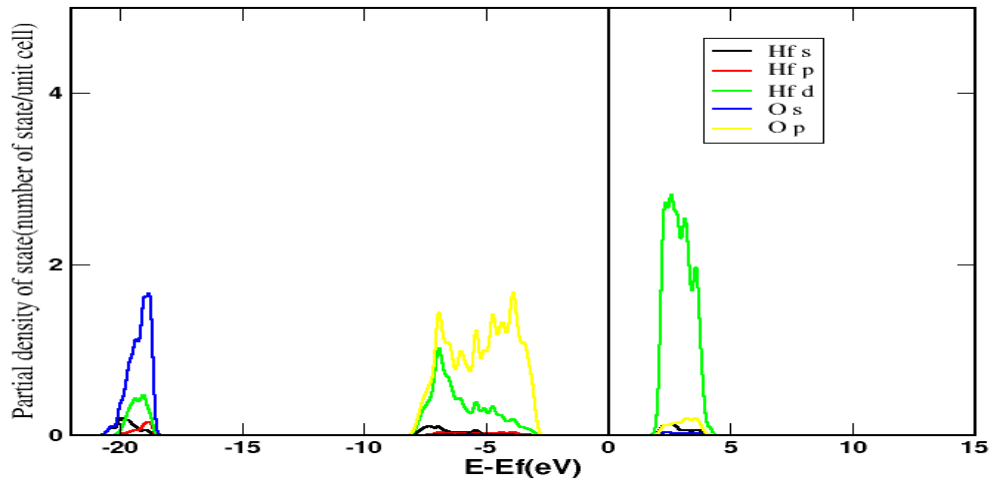


Figure 4. 7 Calculated partial density of (PDOS) pure HfO₂

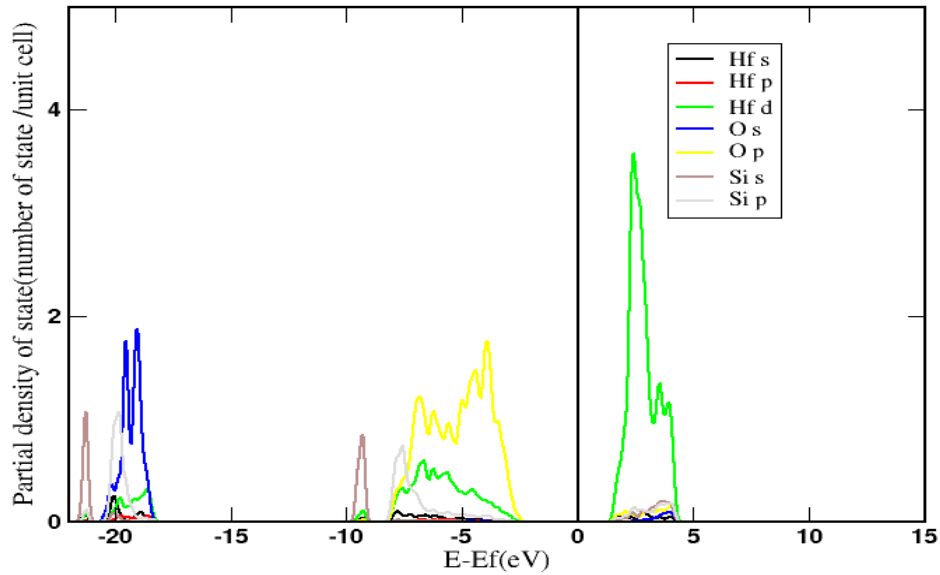


Figure 4. 8 Calculated partial density of Si doped HfO₂

4.5 Born Effective Charge

Born effective charges (BECs) of HfO₂ and Si-doped HfO₂ were computed in the framework of DFT using GGA exchange correlation potential. The Born effective charges Z^* are tensors, defined as the first derivative of polarization with atomic displacement [56]. Born-effective charges play a key role in understanding both the ferroelectric phase and lattice dynamics. The formula described in Eq. 19 is the equation for the "born effective charge properties".

$$Z_{i\alpha\beta} = \frac{\Omega \partial P_{\alpha}}{e \partial u_{i\beta}} \quad (19)$$

Where α and β denote directions, P is the component of the polarization in the α^{th} direction, $U_{i\beta}$ is the periodic displacement of the i^{th} atom in the β^{th} direction, Ω is the unit cell volume, and e is the electron charge. The calculated born effective charge tensors of the atoms for both pure and doped HfO₂ are given below. Born effective charge (BEC or Z^*), sometimes referred to as transverse effective charge or dynamic effective charge [57] is a fundamental quantity that exhibits interaction between lattice displacements and electrostatic fields. For HfO₂ Z^* Born effective

charges for Hf are 5.53329, 5.75256, and 4.73614, and those for oxygen are -2.36111, 2.47285, and -1.95739 in the x, y, and z directions, which agree with the previously calculated value [57]. Z^* of Si is 4.69486, 3.64628, and 3.42116 for $\text{Hf}_{1-x}\text{Si}_x\text{O}_2$. Z^* of Hf are 7.01935, 5.53515, and 4.48271; and Z^* of oxygen are -3.99049, -2.08624, and -1.42006 in the x, y, and z directions. The average value of Z^* on the cations and oxygen is greater for the doped cases compared to pure HfO_2 , and the average value of Z^* increases as the concentration of doping increases, indicating a higher contribution to the dielectric response [58].

4.5.1 Calculated Born effective charge of pure HfO_2

Born effective charge (BEC or, Z^*), also known as transverse or dynamic effective charge, is a fundamental quantity that represents the coupling of lattice displacements and electrostatic fields. The magnitudes of the born effective charges of the Hf and oxygen atoms are greater than their nominal ionic valences (+4 for Hf and -2 for oxygen). The following are the calculated born effective charges of hafnium and oxygen atoms:

$$Z^*(\text{Hf}) = \begin{pmatrix} 5.53329 & -0.24858 & -0.00164 \\ -0.28085 & 5.75256 & -0.00002 \\ -0.00200 & -0.00374 & 4.73614 \end{pmatrix}$$

$$Z^*(\text{O}) = \begin{pmatrix} -2.35648 & -0.83412 & -0.20906 \\ -0.83128 & -2.47230 & 0.76076 \\ -0.05336 & 0.85695 & -1.96461 \end{pmatrix}$$

4.5.2 Born effective charge of silicon doped hafnium oxide

Z^* is equal to the polarization linearly induced by a small displacement of each atom within a zero macroscopic electric field. The magnitudes of the born effective charges after silicon doping are greater than their pure and nominal ionic valences (+4 for Hf and -2 for oxygen), indicating a strong dynamic charge transfer from Hf atoms to O atoms.

$$Z^*(Hf_A) = \begin{pmatrix} 5.86889 & 0.11602 & -0.08707 \\ -0.32612 & 4.73136 & 0.43949 \\ 0.19382 & 0.75740 & 4.53042 \end{pmatrix}$$

$$Z^*(Hf_B) = \begin{pmatrix} 5.95316 & 0.16923 & -0.75406 \\ 0.15280 & 5.93409 & -0.23127 \\ -0.10142 & 0.04749 & 4.65824 \end{pmatrix}$$

$$Z^*(Hf_C) = \begin{pmatrix} 3.19007 & -0.22157 & -0.8497 \\ 0.10094 & 5.31812 & 0.09132 \\ 0.34388 & 0.23854 & 5.76803 \end{pmatrix}$$

$$Z^*(Hf_D) = \begin{pmatrix} 7.01935 & -0.38663 & -0.03886 \\ 0.45527 & 5.53515 & -0.13328 \\ -0.16520 & -0.33122 & 4.48271 \end{pmatrix}$$

$$Z^*(Hf_E) = \begin{pmatrix} 7.10496 & -2.09153 & 1.34053 \\ 0.18955 & 4.94784 & 0.39873 \\ 0.19524 & 0.13180 & 4.64392 \end{pmatrix}$$

$$Z^*(Hf_F) = \begin{pmatrix} 2.05289 & 0.67791 & 0.82090 \\ -0.98544 & 5.66895 & 0.31778 \\ 0.25328 & 0.21468 & 5.27429 \end{pmatrix}$$

$$Z^*(Hf_G) = \begin{pmatrix} 7.01237 & -0.61159 & 0.09633 \end{pmatrix}$$

$$\begin{array}{ccc} -0.01039 & 5.81725 & -0.13547 \\ -0.20123 & -0.11764 & 4.57601 \end{array}$$

$$Z^*(O_A) = \begin{pmatrix} -4.09391 & 1.38007 & 0.42629 \\ 0.45299 & -2.03319 & 0.28459 \\ 0.23578 & 0.10981 & -2.11149 \end{pmatrix}$$

$$Z^*(O_B) = \begin{pmatrix} -1.28755 & -0.58292 & 0.28855 \\ -0.14069 & -2.30108 & -0.46694 \\ -0.30375 & -0.58403 & -2.15763 \end{pmatrix}$$

$$Z^*(O_C) = \begin{pmatrix} -2.62401 & -0.71742 & 0.12860 \\ -0.83564 & -2.73267 & -0.38461 \\ 0.05630 & -0.40930 & -1.80856 \end{pmatrix}$$

$$Z^*(O_D) = \begin{pmatrix} -1.20241 & -0.10976 & -0.55975 \\ 0.10294 & -1.70909 & 0.68906 \\ -1.06235 & 0.35210 & -3.07315 \end{pmatrix}$$

$$Z^*(O_E) = \begin{pmatrix} -3.06659 & 1.31987 & 0.25696 \\ 0.71281 & -2.41536 & 0.75028 \\ 0.11701 & 0.75138 & -1.87328 \end{pmatrix}$$

$$Z^*(O_F) = \begin{pmatrix} -1.23093 & 0.79017 & 0.73377 \\ 0.48179 & -2.34685 & -0.27042 \end{pmatrix}$$

0.35535 -0.42230 -1.92989

$$Z^*(O_G) = \begin{pmatrix} -3.01082 & -0.79914 & -0.09428 \\ -0.70609 & -2.44188 & -0.32965 \\ 0.09295 & -0.39762 & -2.08798 \end{pmatrix}$$

$$Z^*(O_H) = \begin{pmatrix} -3.02906 & -1.22465 & 0.10138 \\ -0.84645 & -2.23048 & 0.84401 \\ 0.08925 & 0.97331 & -1.82588 \end{pmatrix}$$

$$Z^*(O_I) = \begin{pmatrix} -1.72915 & -0.23288 & 0.01003 \\ -0.33205 & -2.18362 & 0.12909 \\ 0.30875 & 0.16504 & -2.13898 \end{pmatrix}$$

$$Z^*(O_J) = \begin{pmatrix} 4.23665 & 1.88637 & 0.90161 \\ 1.28944 & -1.69287 & -0.89487 \\ -0.31116 & -1.11816 & -2.31800 \end{pmatrix}$$

$$Z^*(O_K) = \begin{pmatrix} -3.99049 & 1.73296 & 0.12773 \\ 0.82844 & -2.08624 & -0.71221 \\ 0.28753 & -0.77366 & -1.42006 \end{pmatrix}$$

$$Z^*(O_L) = \begin{pmatrix} -1.77849 & -0.90427 & -0.28582 \\ -0.80677 & -2.73631 & 0.22605 \end{pmatrix}$$

-0.47126 0.39168 -1.71164

$$Z^*(O_M) = \begin{pmatrix} -3.22678 & -1.40478 & -0.23322 \\ -1.03215 & -2.30614 & 0.79740 \\ 0.04401 & 0.92195 & -1.76669 \end{pmatrix}$$

$$Z^*(O_N) = \begin{pmatrix} -3.75502 & 0.39570 & -1.15721 \\ 0.49218 & -1.91822 & -0.82619 \\ -0.25611 & -0.68768 & -1.77465 \end{pmatrix}$$

$$Z^*(O_O) = \begin{pmatrix} -1.83849 & 0.58262 & -0.04553 \\ 0.59494 & -2.28448 & -0.71543 \\ -0.41196 & -0.71013 & -2.40912 \end{pmatrix}$$

$$Z^*(O_P) = \begin{pmatrix} -5.02902 & -0.20148 & -1.17259 \\ 0.06428 & -2.01248 & 0.23302 \\ 0.38810 & 0.50966 & -1.06719 \end{pmatrix}$$

$$Z^*(S_i) = \begin{pmatrix} 4.69486 & 0.37944 & 0.00546 \\ 0.06443 & 3.64628 & -0.09497 \\ 0.28109 & 0.00130 & 3.42116 \end{pmatrix}$$

CHAPTER -FIVE

CONCLUSION AND RECOMMENDATIONS

5.1 Conclusion

The structural, electronic, and born-effective charge properties of doped silicon (Si) were investigated using density functional theory, plane wave basis sets, and ultra-soft pseudo potentials. All calculations have been carried out with the Quantum Espresso package (software). The total minimum energy calculation is performed as a function of cutoff energy and Monk-Horst pack-grid size, respectively, while fixing the other parameters constant. The total energy convergence test is achieved at the energy cutoff of 35 Ry for the first case and at a 5 X 5 X 5 k-point grid size for the second case. The total minimum energy is -3115 Ry for the first case and -3120 Ry for the second case. When we calculate the band structure, it shows an indirect band gap and the band gap of pure monoclinic hafnium oxide at 4.92 eV. This result is in good agreement with other calculations. When silicon is substituted in the site of one hafnium oxide, the band gap is decreased to 4.22 eV and the band moves into the conduction band; also, the band is changed to a direct band gap from an indirect band gap. The cohesive and formation energy formula, used to calculate material stability, shows that the hafnium site is the most stable site to dope silicon atoms because, when we compare after doping silicon atoms into both the Hf and O sites, the Hf site shows a more negative value, indicating a stable site to dope. Each orbital contributes to electronic properties in the density of state calculation, but the Hf d orbital contributes the most in the conduction band and valence band parts, while the O p orbital contributes the most after silicon doping, and the Si s orbital contributes in both parts next to Hf and O. When we compare pure and doped-born effective charges, doped has a large Z^* , which has a great contribution to the dielectric response. The main point for ferroelectric materials is the born-effective charge.

5.2 Recommendations

The ferroelectric material of silicon-doped hafnium oxide needs a lot of study. Based on the result of the study performed in this research, the following recommendations can be made:

- Using large k-points and making the supercell large may give a good result.
- Increasing the concentration of silicon up to an optimum point may give a good result.
- Calculating vibrational and dielectric constant properties needs further study.
- The computational study of rare earth element doping on hafnium oxide needs further study because, most of the time, rare earth element doped hafnium oxide shows large remnant polarization, which is good for non-volatile memory applications.

APPENDICES

Appendix A

1. Running SCF with QUANTUM ESPRESSO

Step 1: SCF calculation and Relax SCF

Step 2: Non-SCF calculation

Step 3: PDOS calculation

The SCF Calculation is performed by running the following command:-

```
$ /usr/bin/mpirun -np 2 /home/Tsega-jit/Documents/code/qe-6.7-ReleasePack/qe6.7/bin/pw.x < HfO2.scf.in > HfO2.scf.out
```

The NSCF Calculation is performed by running the following command:-

```
$ /usr/bin/mpirun -np 2 /home/Tsega-jit/Documents/code/qe-6.7-ReleasePack/qe6.7/bin/pw.x < HfO2.nscf.in > HfO2.nscf.out
```

❖ Step 1: SCF calculation

```
&CONTROL
  Calculation = 'scf'
  restart mode='from_scratch'
  outdir = './tmp'
  prefix = 'hfo'
  pseudo_dir = './'
  tprnfor = .true.
  tstress = .true.
  verbosity = 'high'
/
&SYSTEM

cellldm(1)=9.717440214, cellldm(2)=1.010273381, cellldm(3)=1.035726967
ecutrho = 280
ecutwfc = 35
ibrav = 12
nat = 12
ntyp = 2
occupations = 'smearing'
degauss = 0.001,
```

```

    smearing = 'mv'
/
&ELECTRONS
    mixing_beta = 0.6,
    conv_thr = 1.0d-8,
    diagonalization='david'
    mixing_mode = 'local-TF'
/
ATOMIC_SPECIES
Hf 178.490 Hf.pbe-spn-kjpaw_psl.1.1.0.0.UPF
O 15.9994 O.pbe-n-kjpaw_psl.1.1.0.0.UPF
ATOMIC_POSITIONS crystal
Hf      0.7501900425      0.4999102546      0.3017978773
Hf      0.2498099575      0.9999102546      0.1982021227
Hf      0.2498099575      0.5000897454      0.6982021227
Hf      0.7501900425      0.0000897454      0.8017978773
O       0.5658505851      0.7774535293      0.0970120336
O       0.4341494149      0.2774535293      0.4029879664
O       0.4341494149      0.2225464707      0.9029879664
O       0.5658505851      0.7225464707      0.5970120336
O       0.9346260274      0.2764934161      0.5958442457
O       0.0653739726      0.7764934161      0.9041557543
O       0.0653739726      0.7235065839      0.4041557543
O       0.9346260274      0.2235065839      0.0958442457
K_POINTS automatic
5 5 5 0 0 0

```

❖ Step 2: NSCF calculation

```

&CONTROL
    calculation = 'nscf'
    restart_mode='from_scratch'
    outdir = './tmp'
    prefix = 'hfo'
    pseudo_dir = './'
    tprnfor = .true.
    tstress = .true.
    verbosity = 'high'
/

```

```

&SYSTEM
  celldm(1)=9.717440214, celldm(2)=1.010273381, celldm(3)=1.035726967
  ecutrho = 280
  ecutwfc = 35
 ibrav = 12
  nat = 12
  ntyp = 2
  occupations = 'tetrahedra'
  degauss = 0.001,
  smearing = 'mv'
/
&ELECTRONS
  mixing_beta = 0.6,
  conv_thr = 1.0d-8,
  diagonalization='david'
  mixing_mode = 'local-TF'
/
ATOMIC_SPECIES
Hf 178.490 Hf.pbe-spn-kjpaw_psl.1.1.0.0.UPF
O 15.9994 O.pbe-n-kjpaw_psl.1.1.0.0.UPF
ATOMIC_POSITIONS crystal
Hf      0.7501900425      0.4999102546      0.3017978773
Hf      0.2498099575      0.9999102546      0.1982021227
Hf      0.2498099575      0.5000897454      0.6982021227
Hf      0.7501900425      0.0000897454      0.8017978773
O       0.5658505851      0.7774535293      0.0970120336
O       0.4341494149      0.2774535293      0.4029879664
O       0.4341494149      0.2225464707      0.9029879664

```

O	0.5658505851	0.7225464707	0.5970120336
O	0.9346260274	0.2764934161	0.5958442457
O	0.0653739726	0.7764934161	0.9041557543
O	0.0653739726	0.7235065839	0.4041557543
O	0.9346260274	0.2235065839	0.0958442457

K_POINTS automatic

18 18 18 0 0 0

❖ Step 3 PDOS Calculation

```
&projwfc
  prefix = 'hfo',
  outdir = './tmp',
  ngauss = 0,
  degauss = 0.01,
  Emin = -52,
  Emax = 18,
  DeltaE = 0.001,
  filpdos = 'hfo.pdos.dat'
/
```

Relax Calculation

```
&CONTROL
  calculation = 'relax'
  forc_conv_thr = 0.001
  outdir = './tmp'
  pseudo_dir = './'
/
&SYSTEM

celldm(1)=19.434881194, celldm(2)=0.50513667, celldm(3)=0.510498528
  ecutrho = 280
  ecutwfc = 35
  ibrav = 12
  nat = 24
  ntyp = 3
  occupations = 'smearing'
  degauss = 0.001,
  smearing = 'gaussian'
```

```

/
&ELECTRONS
/
&IONS
ion_dynamics = 'bfgs'
/
  &CELL
    cell_dynamics = 'bfgs',
  /
ATOMIC_SPECIES
Hf 178.490 Hf.pbe-spn-kjpaw_psl.1.1.0.0.UPF
O  15.9994 O.pbe-n-kjpaw_psl.1.1.0.0.UPF
Si 28.0855 Si.pbe-nl-rrkjus_psl.1.1.0.0.UPF
ATOMIC_POSITIONS crystal
Hf  0.362020403      0.457318902      0.292108923
Hf  0.862020373      0.457318902      0.292108923
Hf  0.137979463      0.957318842      0.207890958
Hf  0.637979448      0.957318842      0.207890958
Hf  0.862020373      0.042680990      0.792108834
Hf  0.275556415      0.742602825      0.022291994
Hf  0.637979448      0.542680800      0.707890809
O   0.775556445      0.742602825      0.022291994
O   0.224443451      0.242602959      0.477707922
O   0.724443436      0.242602959      0.477707922
O   0.224443451      0.257396907      0.977707803
O   0.724443436      0.257396907      0.977707803
O   0.275556415      0.757396817      0.522291839
O   0.775556445      0.757396817      0.522291839
O   0.466075420      0.330121905      0.652905822
O   0.966075420      0.330121905      0.652905822
O   0.033924490      0.830121815      0.847093821
O   0.533924460      0.830121815      0.847093821
O   0.033924490      0.669877827      0.347093910
O   0.533924460      0.669877827      0.347093910
O   0.466075420      0.169877961      0.152905956
O   0.966075420      0.169877961      0.152905956
O   0.137979463      0.542680800      0.707890809
Si  0.362020403      0.042680990      0.792108834
K_POINTS automatic
5 5 5 0 0 0

```

Appendix B

2. Running SCF calculation for supercells using Quantum ESPRESSO.

```
&CONTROL
  calculation = 'scf'
  restart_mode='from_scratch'
  outdir = './tmp'
  prefix = 'hfo'
  pseudo_dir = './'
  tprnfor = .true.
  tstress = .true.
  verbosity = 'high'
/
&SYSTEM
  cellldm(1)=19.434881194, cellldm(2)=0.50513667,cellldm(3)=0.510498528
  ecutrho = 280
  ecutwfc = 35
 ibrav = 12
  nat = 24
  ntyp = 3
  occupations = 'smearing'
  degauss = 0.001,
  smearing = 'mv'
/
&ELECTRONS
  mixing_beta = 0.6,
  conv_thr = 1.0d-8,
  diagonalization='david'
  mixing_mode = 'local-TF'
```

```

/
ATOMIC_SPECIES
Hf 178.490 Hf.pbe-spn-kjpaw_psl.1.0.0.UPF
O 15.9994 O.pbe-n-kjpaw_psl.1.0.0.UPF
Si 28.0855 Si.pbe-nl-rrkjus_psl.1.0.0.UPF
ATOMIC_POSITIONS (crystal)
Hf 0.3636877657 0.4402633411 0.3210430122
Hf 0.8913266010 0.5168662055 0.2759575649
Hf 0.1376072717 1.0088868823 0.2232650012
Hf 0.6470324631 0.9417597594 0.2189116939
Hf 0.8867962942 0.0066848988 0.7606287253
Hf 0.1385211518 0.5540510767 -0.2748882252
Hf 0.6366462458 0.4886386117 0.6958718070
O 0.7576632418 0.6831757339 0.0217686430
O 0.2060422331 0.2565534765 0.4827069068
O 0.7338410063 0.2572765376 0.3970635417
O 0.2431873565 0.3939407688 1.0137293776
O 0.7161402908 0.1651365321 0.8857067916
O 0.2536405926 0.7371544546 0.4538710779
O 0.7653982379 0.7509310399 0.5238277991
O 0.4578604299 0.2254193403 0.6472734217
O 0.9654481719 0.3346088650 0.6125476319
O 0.2660640808 0.9045111516 0.9321017222
O 0.5146747169 0.7543923559 0.8826797491
O 0.0082414740 0.8084273262 0.4666288209
O 0.5312327029 0.6467714152 0.3894381702
O 0.4736937014 0.1543954216 0.1348553754
O 0.9776014995 0.2156793021 0.0925889917
O 0.0117409337 0.7442926102 0.9712405568
Si 0.4159099847 0.0101799929 0.8711790250

K_POINTS automatic
5 5 5 0 0 0

```

Appendix C

3. Calculating born effective charge

Step 1: SCF calculation

Step 2: ph. calculation

Ph calculation for born effective after SCF calculation

```
&inputph
 outdir="./tmp/",
  prefix="hfo",
  tr2_ph=1d-14,
  ldisp=.false.,
  epsil=.true.,
  amass(1)=178.49, amass(2)=15.9994,
  fildyn='hfo.dyn',
/
0.0  0.0  0.0
```

References

- [1] K. M. Rabe, M. Dawber, C. Lichtensteiger, C. H. Ahn, and J.-M. M. Triscone, “Modern Physics of Ferroelectrics: Essential Background BT - Physics of Ferroelectrics: A Modern Perspective,” *Top. Appl. Phys.*, vol. 105, no. 2007, pp. 1–30, 2007, [Online]. Available: http://dx.doi.org/10.1007/978-3-540-34591-6_1
- [2] C. Richter, T. Schenk, and MH Park, “Si Doped Hafnium Oxide—A ‘Fragile’ Ferroelectric System,” *Adv. Electron. Mater.*, vol. 3, no. 10, pp. 1–12, 2017, doi: 10.1002/aelm.201700131.
- [3] D. Damjanovic, “Ferroelectric, dielectric and piezoelectric properties of ferroelectric thin films and ceramics,” *Reports Prog. Phys.*, vol. 61, no. 11, pp. 1267–1324, 1998, doi: 10.1088/0034-4885/61/9/002.
- [4] R. D. King-Smith and D. Vanderbilt, “Theory of polarization of crystalline solids,” *Phys. Rev. B*, vol. 47, no. 3, pp. 1651–1654, 1993, doi: 10.1103/PhysRevB.47.1651.
- [5] S. Shao, J. Zhang, Z. Zhang, P. Zheng, “High piezoelectric properties and domain configuration in BaTiO₃ ceramics obtained through the solid-state reaction route,” *J. Phys. D: Appl. Phys.*, vol. 41, no. 12, p. 125408, 2008.
- [6] G. Philippot, C. Elissalde, M. Maglione, and C. Aymonier, “Supercritical fluid technology: A reliable process for high quality BaTiO₃ based nanomaterials,” *Adv. Powder Technol.*, vol. 25, no. 5, pp. 1415–1429, 2014, doi: 10.1016/j.appt.2014.02.016.
- [7] J. Wang, H. P. Li, and R. Stevens, “Hafnia and hafnia-toughened ceramics,” *J. Mater. Sci.*, vol. 27, no. 20, pp. 5397–5430, 1992.
- [8] J. M. Leger, A. Atouf, P. E. Tomaszewski, and A. S. Pereira, “Pressure-induced phase transitions and volume changes in HfO₂ up to 50 GPa,” *Phys. Rev. B*, vol. 48, no. 1, pp. 93–98, 1993, doi: 10.1103/PhysRevB.48.93.
- [9] M. Hyuk Park, H. Joon Kim, Y. Jin Kim, W. Lee, T. Moon, and C. Seong Hwang, “Evolution of phases and ferroelectric properties of thin Hf_{0.5}Zr_{0.5}O₂ films according to the thickness and annealing temperature,” *Appl. Phys. Lett.*, vol. 102, no. 24, pp. 0–5, 2013, doi: 10.1063/1.4811483.
- [10] J. E. Lowther, J. K. Dewhurst, J. M. Leger, and J. Haines, “Relative stability of ZrO₂ and HfO₂ structural phases,” *Phys. Rev. B*, vol. 60, no. 21, pp. 14485–14488, 1999, doi: 10.1103/physrevb.60.14485.
- [11] C. E. CURTIS, L. M. DONEY, and J. R. JOHNSON, “Some Properties of Hafnium Oxide, Hafnium Silicate, Calcium Hafnate, and Hafnium Carbide,” *J. Am. Ceram. Soc.*, vol. 37, no. 10, pp. 458–465, 1954, doi: 10.1111/j.1151-2916.1954.tb13977.x.
- [12] Z. Fan, J. Chen, and J. Wang, “Ferroelectric HfO₂-based materials for next-generation ferroelectric memories,” *J. Adv. Dielectr.*, vol. 6, no. 2, pp. 1–11, 2016, doi:

10.1142/S2010135X16300036.

- [13] R. J. D. Tilley, *Understanding solids: the science of materials*. John Wiley & Sons, 2004.
- [14] X. Hao, “A review on the dielectric materials for high energy-storage application,” *J. Adv. Dielectr.*, vol. 03, no. 01, p. 1330001, 2013, doi: 10.1142/s2010135x13300016.
- [15] J. C. Burfoot and G. W. Taylor, *Polar dielectrics and their applications*. Univ of California Press, 2022.
- [16] J.F Scott, L. Kammerdiner, M. Parris, S. Traynor, “Switching kinetics of lead zirconate titanate submicron thin-film memories,” *J. Appl. Phys.*, vol. 64, no. 2, pp. 787–792, 1988, doi: 10.1063/1.341925.
- [17] K. OKAZAKI and K. NAGATA, “Effects of Grain Size and Porosity on Electrical and Optical Properties of PLZT Ceramics,” *J. Am. Ceram. Soc.*, vol. 56, no. 2, pp. 82–86, 1973, doi: 10.1111/j.1151-2916.1973.tb12363.x.
- [18] M. Takahashi, “Space charge effect in lead zirconate titanate ceramics caused by the addition of impurities,” *Jpn. J. Appl. Phys.*, vol. 9, no. 10, pp. 1236–1246, 1970, doi: 10.1143/JJAP.9.1236.
- [19] P. D. Beale and H. M. Duiker, “Grain-size effects in ferroelectric switching,” *Ferroelectrics*, vol. 117, no. 1, pp. 165–170, 1991, doi: 10.1080/00150199108222414.
- [20] D. A. Buck, “Ferroelectrics for Digital Information Storage and Switching.,” MASSACHUSETTS INST OF TECH CAMBRIDGE DIGITAL COMPUTER LAB, 1952.
- [21] L. Van Hai, M. Takahashi, and S. Sakai, “Downsizing of ferroelectric-gate field-effect-transistors for ferroelectric-NAND flash memory cells,” *2011 3rd IEEE Int. Mem. Work. IMW 2011*, no. August, 2011, doi: 10.1109/IMW.2011.5873239.
- [22] T. S. Böske, J. Müller, D. Bräuhäus, U. Schröder, and U. Böttger, “Ferroelectricity in hafnium oxide thin films,” *Appl. Phys. Lett.*, vol. 99, no. 10, 2011, doi: 10.1063/1.3634052.
- [23] E. Pavoni, E. Mohebbi, P. Stipa, D. Mencarelli, L. Pierantoni, and E. Laudadio, “The Role of Zr on Monoclinic and Orthorhombic $\text{Hf}_x\text{Zr}_y\text{O}_2$ Systems : A First-Principles Study,” 2022.
- [24] A. Debernardi, “ Ab initio study of structural, vibrational and dielectric properties of high- κ HfO_2 as a function of doping ,” *IOP Conf. Ser. Mater. Sci. Eng.*, vol. 8, p. 012021, 2010, doi: 10.1088/1757-899x/8/1/012021.
- [25] E. Garfunkel and E. Gusev, *Fundamental aspects of ultrathin dielectrics on Si-based devices*, vol. 47. Springer Science & Business Media, 2012.
- [26] J. Robertson and R. M. Wallace, “High-K materials and metal gates for CMOS

- applications,” *Mater. Sci. Eng. R Reports*, vol. 88, pp. 1–41, 2015.
- [27] L.G Wang, Y. Xiong, W. Xiao, L. Cheng, J. Du, “doped HfO₂ Computational investigation of the phase stability and the electronic properties for Gd-doped HfO₂,” vol. 201903, pp. 0–4, 2014, doi: 10.1063/1.4878401.
- [28] L. H. D. S. Lacerda and S. R. De Lazaro, “Ba-Doped ZnO materials: A DFT simulation to investigate the doping effect on ferroelectricity,” *Quim. Nova*, vol. 39, no. 3, pp. 261–266, 2016, doi: 10.5935/0100-4042.20160023.
- [29] M. Rizwan, I. Zeba, M. Shakil, and S. S. A. Gillani, “Optik Electronic , structural and optical properties of BaTiO₃ doped with lanthanum (La): Insight from DFT calculation,” *Opt. - Int. J. Light Electron Opt.*, vol. 211, no. February, p. 164611, 2020, doi: 10.1016/j.ijleo.2020.164611.
- [30] M. Lederer, R. Olivo, D. Lehninger , “On the Origin of Wake-Up and Antiferroelectric-Like Behavior in Ferroelectric Hafnium Oxide,” *Phys. Status Solidi - Rapid Res. Lett.*, vol. 15, no. 5, pp. 1–8, 2021, doi: 10.1002/pssr.202100086.
- [31] U. Schroeder, C. Richter, MH. Park, and T. Schenk “Lanthanum-Doped Hafnium Oxide: A Robust Ferroelectric Material,” *Inorg. Chem.*, vol. 57, no. 5, pp. 2752–2765, 2018, doi: 10.1021/acs.inorgchem.7b03149.
- [32] K. Rahmanizadeh, “Ferroelectric Materials with Interfaces : First Principles Calculations,” pp. 1–109, 2011, [Online]. Available: http://www.fz-juelich.de/SharedDocs/Downloads/PFI/PFI-1/EN/Rahmanizadeh.PhD_pdf.pdf?__blob=publicationFile
- [33] L. J. Sham, “Density functional theory,” *Phys. Today*, vol. 35, no. 2, pp. 36–43, 1982, doi: 10.1063/1.2914933.
- [34] J. F. Scott, “Applications of modern ferroelectrics,” *Science (80-.)*, vol. 315, no. 5814, pp. 954–959, 2007, doi: 10.1126/science.1129564.
- [35] H. Boubekeur, “Contamination Aspects in Integrating High Dielectric Constant and Ferroelectric Materials into CMOS Processes DOKTOR-INGENIEUR Hocine Boubekeur,” 2002.
- [36] B. O. Xiao, “Growth characterization and applications of multifunctional ferroelectric thin films,” *Virginia Commonw. Univ.*, vol. 15, no. 5, p. NP, 2009, [Online]. Available: <http://www.ncbi.nlm.nih.gov/pubmed/23572506>
- [37] J. M. Smith, S. P. Jones, and L. D. White, “Rapid Communication,” *Gastroenterology*, vol. 72, no. 1, p. 193, 1977, doi: 10.1016/S0016-5085(77)80340-5.
- [38] S. Baroni, A. Dal Corso, S. De Gironcoli, and P. Giannozzi “Quantum ESPRESSO: open-source package for research in electronic structure, simulation, and optimization,” *Code available from http://www.quantum-espresso.org*, 2005.

- [39] W. E. Pickett, "Pseudopotential methods in condensed matter applications," *Comput. Phys. Reports*, vol. 9, no. 3, pp. 115–197, 1989, doi: 10.1016/0167-7977(89)90002-6.
- [40] P. Giannozzi, S. Baroni, N. Bonini, M. Calandra, and R. Car, "QUANTUM ESPRESSO: A modular and open-source software project for quantum simulations of materials," *J. Phys. Condens. Matter*, vol. 21, no. 39, 2009, doi: 10.1088/0953-8984/21/39/395502.
- [41] G. Samsonidze and B. Kozinsky, "Accelerated Screening of Thermoelectric Materials by First-Principles Computations of Electron–Phonon Scattering," *Adv. Energy Mater.*, vol. 8, no. 20, pp. 1–10, 2018, doi: 10.1002/aenm.201800246.
- [42] F. Furche, "Molecular tests of the random phase approximation to the exchange–correlation energy functional," *Phys. Rev. B - Condens. Matter Mater. Phys.*, vol. 64, no. 19, pp. 1–8, 2001, doi: 10.1103/PhysRevB.64.195120.
- [43] J. P. Perdew and A. Zunger, "Self-interaction correction to density-functional approximations for many-electron systems," *Phys. Rev. B*, vol. 23, no. 10, pp. 5048–5079, 1981, doi: 10.1103/PhysRevB.23.5048.
- [44] J. P. Perdew, "Accurate Density Functional for the Energy: Real-Space Cutoff of the Gradient Expansion for the Exchange Hole," *Phys. Rev. Lett.*, vol. 55, no. 16, pp. 1665–1668, 1985, doi: 10.1103/PhysRevLett.55.1665.
- [45] "First principles characterisation of defects in irradiated graphitic materials A thesis submitted towards fulfilment of the requirement for University of Sussex School of Life Sciences," no. September, 2015.
- [46] M. G. Trisolini, J. Cromwell, and G. C. Pope, "Conclusions: Planning for Second-Generation Pay for Performance," *Pay Perform. Heal. Care Methods Approaches*, no. June, pp. 341–370, 2011, doi: 10.3768/rtipress.2011.bk.0002.1103.12.
- [47] E. I. Proynov, E. Ruiz, A. Vela, and D. R. Salahub, "Determining and extending the domain of exchange and correlation functionals," *Int. J. Quantum Chem.*, vol. 56, no. 29 S, pp. 61–78, 1995, doi: 10.1002/qua.560560808.
- [48] P. Muller, "Practical suggestions for better crystal structures," *Crystallogr. Rev.*, vol. 15, no. 1, pp. 57–83, 2009, doi: 10.1080/08893110802547240.
- [49] R. J. Slager, A. Mesaros, V. Juričić, and J. Zaanen, "The space group classification of topological band-insulators," *Nat. Phys.*, vol. 9, no. 2, pp. 98–102, 2013, doi: 10.1038/nphys2513.
- [50] Q. He, B. Yu, Z. Li, and Y. Zhao, "Density Functional Theory for Battery Materials," *Energy Environ. Mater.*, vol. 2, no. 4, pp. 264–279, 2019, doi: 10.1002/eem2.12056.
- [51] T. Tan, Z. Liu, and Y. Li, "First-principles calculations of electronic and optical properties of Ti-doped monoclinic HfO₂," *J. Alloys Compd.*, vol. 510, no. 1, pp. 78–82, 2012, doi: <https://doi.org/10.1016/j.jallcom.2011.08.084>.

- [52] C. Song and H. J. Kwon, “Ferroelectrics based on hfo2 film,” *Electron.*, vol. 10, no. 22, pp. 1–19, 2021, doi: 10.3390/electronics10222759.
- [53] A. Mostefai, S. Berrah, and H. Abid, “Electronics properties of monoclinic HfO₂,” *J. Nano- Electron. Phys.*, vol. 10, no. 6, pp. 6–9, 2018, doi: 10.21272/jnep.10(6).06026.
- [54] X. Gonze and C. Lee, “Dynamical matrices, Born effective charges, dielectric permittivity tensors, and interatomic force constants from density-functional perturbation theory,” *Phys. Rev. B - Condens. Matter Mater. Phys.*, vol. 55, no. 16, pp. 10355–10368, 1997, doi: 10.1103/PhysRevB.55.10355.
- [55] M. Kamruzzaman, M. A. Helal, I. E. Ara, A. K. M. Farid Ul Islam, and M. M. Rahaman, “A comparative study based on the first principles calculations of ATiO₃ (A = Ba, Ca, Pb and Sr) perovskite structure,” *Indian J. Phys.*, vol. 90, no. 10, pp. 1105–1113, 2016, doi: 10.1007/s12648-016-0848-3.
- [56] A. Roy, R. Prasad, S. Auluck, and A. Garg, “First-Principles Calculations of Born Effective Charges and Spontaneous Polarization of Ferroelectric Bismuth Titanate,” pp. 1–36.
- [57] Y. Zhang, H. X. Chen, L. Duan, J. Bin Fan, L. Ni, and V. Ji, “A comparison study of the Born effective charges and dielectric properties of the cubic, tetragonal, monoclinic, ortho-I, ortho-II and ortho-III phases of zirconia,” *Solid State Sci.*, vol. 81, pp. 58–65, 2018, doi: 10.1016/j.solidstatesciences.2018.05.005.
- [58] G. Dutta, “A first-principles study of enhanced dielectric responses in Ti and Ce doped HfO₂ A first-principles study of enhanced dielectric responses in Ti and Ce,” vol. 012907, no. May 2013, 2009, doi: 10.1063/1.3063126.